AFFTC-PA-11133

Space-Time Coding For Aeronautical Telemetry: Part I — System Description

Michael Rice

AIR FORCE FLIGHT TEST CENTER
EDWARDS AFB, CA

6/2/2011

Approved for public release; distribution is unlimited.

AIR FORCE FLIGHT TEST CENTER
EDWARDS AIR FORCE BASE, CALIFORNIA
AIR FORCE MATERIEL COMMAND
UNITED STATES AIR FORCE

AFFTC

REPORT DOCUMENTATION PAGE

Form Approved
OMB No. 0704-0188

1. REPORT DATE *(DD-MM-YYYY)*	**2. REPORT TYPE**	**3. DATES COVERED** *(From - To)*
02-06-2011	Technical Brief	June 11 – Oct 11

4. TITLE AND SUBTITLE

Space-Time Coding For Aeronautical Telemetry: Part I — System Description

5a. CONTRACT NUMBER

5b. GRANT NUMBER

5c. PROGRAM ELEMENT NUMBER

6. AUTHOR(S)

Michael Rice

5d. PROJECT NUMBER

5e. TASK NUMBER

5f. WORK UNIT NUMBER

7. PERFORMING ORGANIZATION NAME(S) AND ADDRESS(ES) AND ADDRESS(ES)

Brigham Young University, Provo, Utah, USA

8. PERFORMING ORGANIZATION REPORT NUMBER

AFFTC-PA-11133

9. SPONSORING / MONITORING AGENCY NAME(S) AND ADDRESS(ES)

Tom Young, EA
AFMC, AFFTC, 412 Test Wing
Edwards AFB CA 93524

10. SPONSOR/MONITOR'S ACRONYM(S)

N/A

11. SPONSOR/MONITOR'S REPORT NUMBER(S)

12. DISTRIBUTION / AVAILABILITY STATEMENT

Approved for public release A: distribution is unlimited.

13. SUPPLEMENTARY NOTES

CA: Air Force Flight Test Center Edwards AFB CA CC: 012100

14. ABSTRACT

This paper described the design and implementation of a prototype transmitter and a prototype demodulator/decoder for space-time coded SOQPSK-TG for aeronautical telemetry. The design exercise showed that the space-time coding concept can be reduced to hardware. The laboratory bit error rate tests showed that the performance of the prototype demodulator in a 2-transmit/1-receive antenna configuration is comparable to that of existing SOQPSK demodulators in a 1-transmit/1- receive antenna configuration.

15. SUBJECT TERMS

Space-time coding; SOQPSK; SOQPSK-TG; aeronautical telemetry; aircraft antenna;

16. SECURITY CLASSIFICATION OF: **Unclassified**			**17. LIMITATION OF ABSTRACT**	**18. NUMBER OF PAGES**	**19a. NAME OF RESPONSIBLE PERSON**
a. REPORT	**b. ABSTRACT**	**c. THIS PAGE**			412 TENG/EN (Tech Pubs)
Unclassified	Unclassified	Unclassified	None	16	**19b. TELEPHONE NUMBER** *(include area code)* 661-277-8615

SPACE-TIME CODING FOR AERONAUTICAL TELEMETRY: PART I — SYSTEM DESCRIPTION

Michael Rice
Brigham Young University
Provo, Utah, USA

ABSTRACT

This paper described the design and implementation of a prototype transmitter and a prototype demodulator/decoder for space-time coded SOQPSK-TG for aeronautical telemetry. The design exercise showed that the space-time coding concept can be reduced to hardware. The laboratory bit error rate tests showed that the performance of the prototype demodulator in a 2-transmit/1-receive antenna configuration is comparable to that of existing SOQPSK demodulators in a 1-transmit/1-receive antenna configuration.

INTRODUCTION

Historically, air-to-ground telemetry links comprise a transmit antenna mounted on the underside of the fuselage and a fixed ground station equipped with a tracking antenna as illustrated in Figure 1 (a). However, aircraft maneuvers tend to place the place the fuselage in between the transmit antenna and receive antenna thus blocking the line-of-sight propagation path as illustrated in Figure 1 (b). The traditional solution has been the use of two antennas to transmit the same signal. The typical configuration uses one antenna mounted on the bottom of the fuselage and a second antenna mounted on the top of the fuselage. As illustrated in Figure 1 (c), when the line-of-sight propagation from the bottom antenna to the ground station is blocked, line-of-sight propagation from the top antenna is unobstructed and the link is maintained.

Because the two antennas are separated in space, the two signals arrive at the ground station with different phases. This is not a problem when only one of the signals has an unobstructed line-of-sight propagation path to the ground station. When both signals have an unobstructed line-of-site propagation path to the ground station, some unintended behavior is observed. For certain aspect angles, the phases of the two signals are such that the signals reinforce each other. However, for other aspect angles, the phases of the two signals are such that the signals cancel (or nearly cancel). As a consequence, the two-transmit antenna system behaves as a single composite antenna with an undesirable gain pattern as illustrated in Figure 1 (d).

Several solutions to this problem have been considered.

1. One obvious solution is to use different carrier frequencies for the two antennas. While simple, this solution requires twice the bandwidth and can claim the use of two ground station antennas. The current challenges with spectrum allocations for telemetry are well-known — solutions that require *more* bandwidth are unworkable.

2. Another solution is to equip the aircraft with a steerable antenna and a mechanism for pointing the transmitted signal directly at the ground station. This family of solutions requires sophisticated antenna technology to implement electronically steerable antennas and a provision for computing the steering vectors: either an uplink signal used to correct errors in the steering vector or onboard computation based on TSPI and the ground station location.

3. The solutions described in this paper is the use if *transmit diversity*. Transmit diversity applies two *different*, but related, signals to the two transmit antennas. The relationship between the two signals is defined by a *space-time code* [1] – [3]. The space-time code is designed so that the instantaneous phase relationship of the two signals is adjusted to avoid destructive interference when averaged over the length of the block code. In addition, all data can be recovered when only one of the two transmitted signals is available at the receiver. In comparison with the other solutions described above, this solution does not require additional spectrum and places only modest complexity increases (to be described below) on the airborne platform. The complexity is concentrated in the ground station, where size and weight are less important.

To test the space-time coding approach using real hardware in actual test flight scenarios, a prototype modulator and demodulator were designed and used in experiments at the Air Force Flight Test Center. This paper describes the prototype system. The results of the test flights are described in the "companion paper" [4].

TRANSMITTER

A block diagram of the space-time coded transmitter is illustrated in Figure 2. As with almost all telemetry transmitters, this modulator accepts a bit stream (NRZ-L) and a corresponding clock as its inputs. The input data bits are encoded using a space-time encoder and 128 pilot bits are inserted for every 3200 coded bits as illustrated in Figure 3. The multiplexed data and pilot bits are applied to two SOQPSK-TG modulators with differential encoding *disabled*.

The operation of the bit-level space-time encoder is as follows. Given an input bit sequence $b_0, b_1, \ldots$, the encoder groups the bits into non-overlapping segments of 4 bits each:

$$b_0, b_1, b_2, b_3 | b_4, b_5, b_6, b_7 | \ldots | b_{4k}, b_{4k+1}, b_{4k+2}, b_{4k+3} | \ldots \tag{1}$$

Bit stream A is defined by

$$b_0, b_1, \overline{b}_2, b_3 | b_4, b_5, \overline{b}_6, b_7 | \ldots | b_{4k}, b_{4k+1}, \overline{b}_{4k+2}, b_{4k+3} | \ldots \tag{2}$$

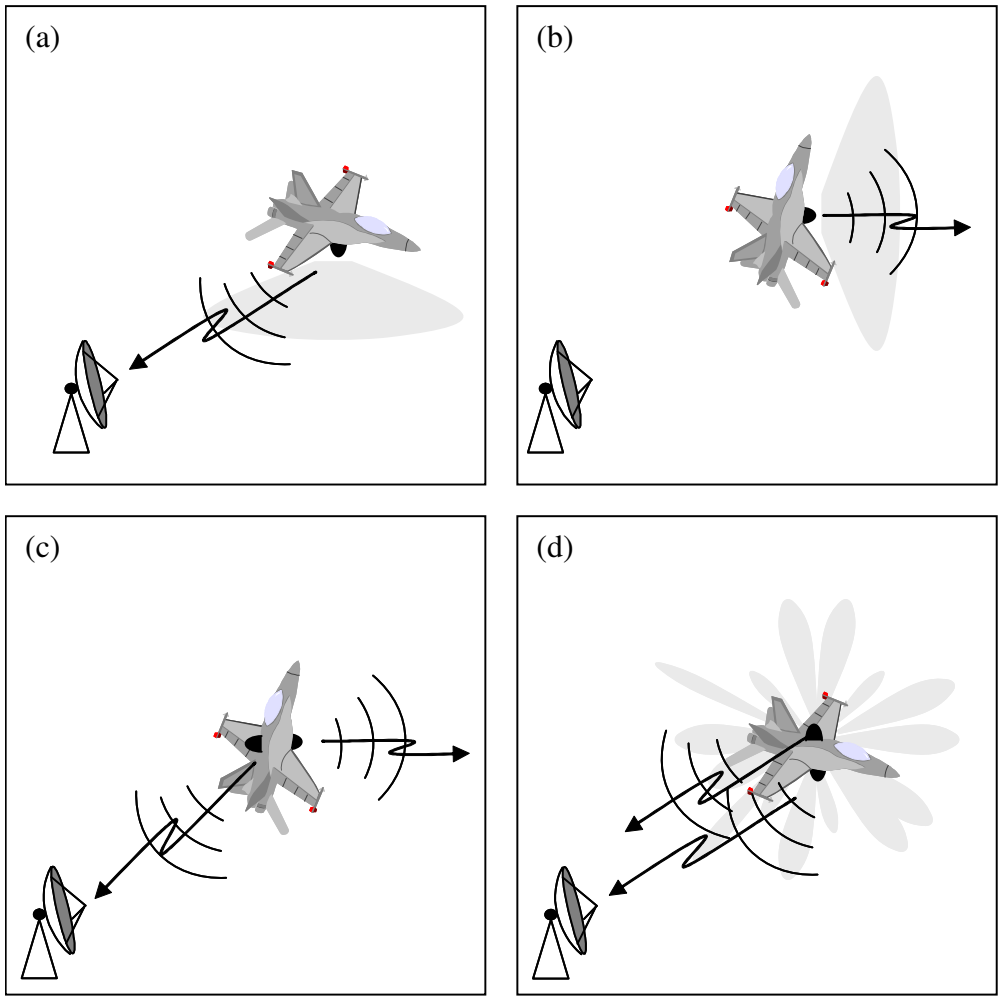

Figure 1: Illustration of the basic problem of dual-antenna air-to-ground communication: (a) the air-to-ground link for normal, level flight; (b) line-of-sight propagation from a single antenna can be blocked during maneuvers; (c) the use of two transmit antennas can solve this coverage problem; (d) when the same signal is transmitted from both antennas, self-interference results and has the same effect as a composite antenna with a very poor beam pattern.

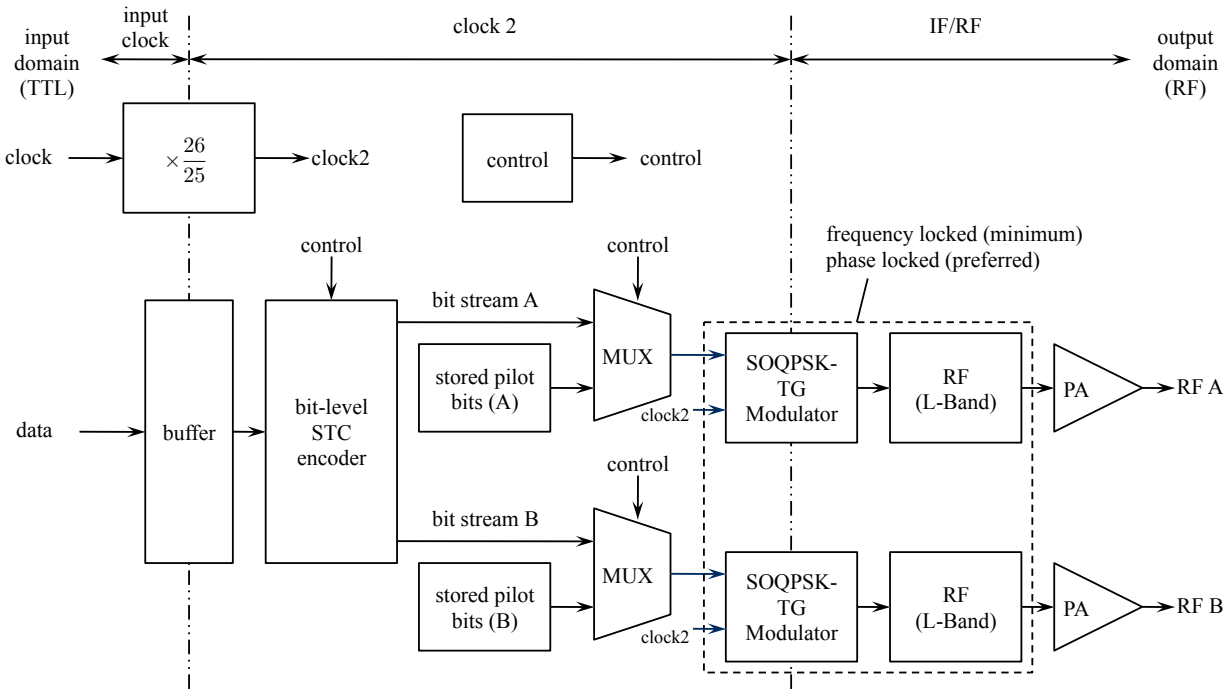

Figure 2: A block diagram of the STC modulator.

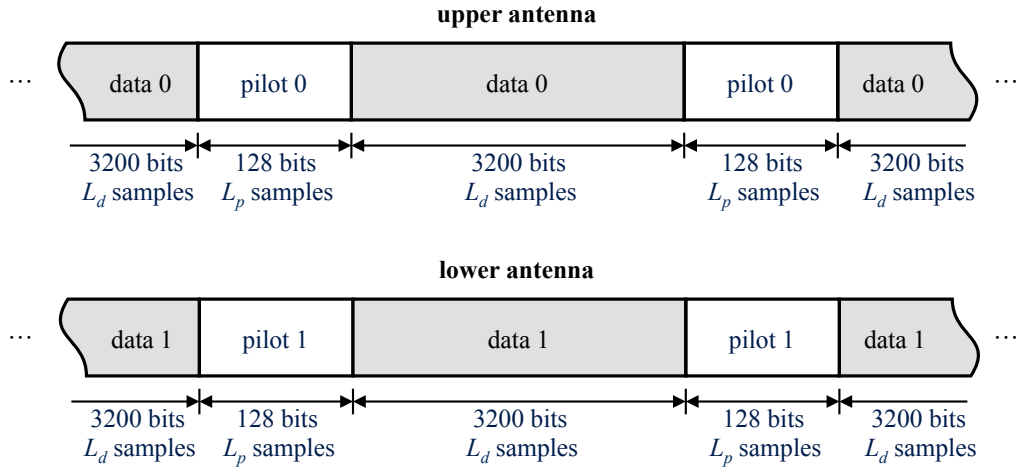

Figure 3: The relationship between the data and pilot bits used for the space-time coded system.

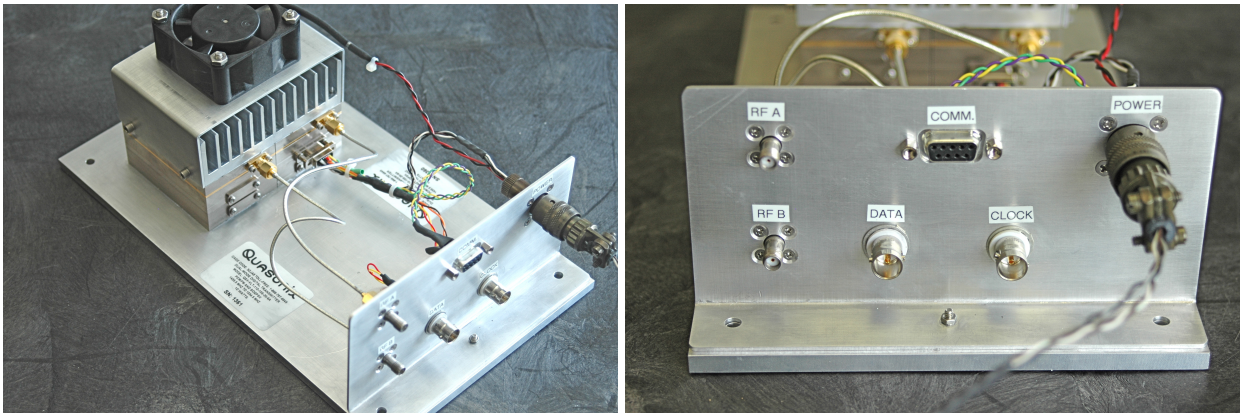

Figure 4: Images of the prototype space-time coded transmitter.

where $\overline{b}_i$ means the logical complement of bit b_i and bit stream B is defined by

$$b_2, b_3, b_0, \overline{b}_1 | b_6, b_7, b_4, \overline{b}_5 | \ldots | b_{4k+2}, b_{4k+3}, b_{4k}, \overline{b}_{4k+1} | \ldots . \tag{3}$$

Pilot bit insertion is accomplished using the two different pilot bit sequences stored in a pair of memory elements, a pair of multiplexors, and a clock operating at frequency 26/25 times the input clock frequency. Observe that the pilot bit insertion increases the bit rate by a factor of

$$\frac{3200 + 128}{3200} = 1.04$$

or 4%. The purpose of the pilot bits is to estimate the frequency offset, delays, gains, and phase shifts as described in the next section.

Two RF outputs are produced by the space-time modulator: one for each transmit antenna. The SOQPSK-TG modulators used to produce the RF signals should be frequency locked at a minimum. The prototype modulator designed for this project produced a pair of 10-W L-band signals. Images of the prototype modulator designed for this project are illustrated in Figure 4.

DEMODULATOR

Let $\cos(\omega_{\text{IF}} t + \phi_0(t))$ and $\cos(\omega_{\text{IF}} t + \phi_1(t))$ be the real-valued band-pass versions of the SOQPSK-TG signals transmitted from antennas 0 and 1, respectively. Here, $\omega_{\text{IF}} = 2\pi f_{\text{IF}}$ where f_{IF} is the intermediate frequency (IF) in Hz. The received IF signal is

$$r_{\text{IF}}(t) = |h_0| \cos([\omega_{\text{IF}} + \omega_0]t + \phi_0(t - \tau_0) + \theta_0) + |h_1| \cos([\omega_{\text{IF}} + \omega_0]t + \phi_1(t - \tau_1) + \theta_1) + w_{\text{IF}}(t) \tag{4}$$

where $|h_0|$ and $|h_1|$ are the gains between transmit antennas 0 and 1, respectively, and the receive antenna; θ_0 and θ_1 are the phase shifts between transmit antennas 0 and 1, respectively, and the receive antenna; τ_0 and τ_1 are the delays between the transmit antennas 0 and 1, respectively, and the receive antenna; and $\omega_0 = 2\pi f_0$ where f_0 is an unknown frequency offset in Hz. Using an

I/Q mixer and a pair of low-pass filters, the complex-valued low-pass equivalent version of the received signal is

$$r(t) = \Big[h_0 s_0(t-\tau_0) + h_1 s_1(t-\tau_1)\Big]\, e^{j\omega_0 t} + w(t) \tag{5}$$

where $s_0(t) = e^{j\phi_0(t)}$ and $s_1(t) = e^{j\phi_1(t)}$ are the complex baseband versions of the SOQPSK-TG signals transmitted from antennas 0 and 1, respectively; $h_0 = |h_0|e^{j\theta_0}$ and $h_1 = |h_1|e^{j\theta_1}$ are the complex-valued channel gains (magnitude and phase) between transmit antennas 0 and 1 and the receive antenna, respectively; $w(t)$ is the complex-baseband version of the real-valued bandpass thermal noise term $w_{\text{IF}}(t)$; and τ_0, τ_1 and ω_0 are defined above. The pilot bits are used to estimate the parameters h_0, h_1, τ_0, τ_1, and ω_0. To do so, the position of the samples corresponding to the pilot symbols known. Thus, demodulation and decoding proceed as follows:

1. Find the position of the samples corresponding to the pilot bits in the received data.
2. Estimate the frequency offset ω_0 and the channel parameters h_0, h_1, τ_0, τ_1. This estimator is recursive in the sense that estimates for the frequency offset depend on the channel parameter estimates, and vice versa. The recursion used to compute the estimates is as follows:
   (a) Set $\hat{h}_0 = 1$, $\hat{h}_1 = 1$, $\tau_0 = 0$ and $\tau_1 = 0$.
   (b) Compute the estimate for the frequency offset based on the estimates $\hat{h}_0$, $\hat{h}_1$, $\hat{\tau}_0$, and $\hat{\tau}_1$.
   (c) Compute estimates for the channel parameters based on the estimate $\hat{\omega}_0$.
   (d) Go to step (b).

   The (b) – (d) cycle is performed three times.
3. Apply a detection filter, adjust the timing of the received signal by the delays $\hat{\tau}_0$ and $\hat{\tau}_1$, and downsample to 1 sample/bit.
4. Perform demodulation and decoding using the Viterbi Algorithm operating on the trellis defined by the SOQPSK-TG state transitions and the space-time code.

Note that in steady-state operation, Step 1 does not need to be performed. However, the prototype demodulator continues to track the position of the pilot bit samples. A sudden large change in the position of the pilot bit samples is an indication that either the demodulator has lost frame synchronization or something has gone terribly wrong in the transmitter.

A block diagram of the prototype demodulator implementation of this algorithm is illustrated in Figure 5. The elements in the block diagram are described below.

Sampling, Downconversion, and Resampling The received IF signal (4) is sampled at a rate of $93\,{}^1\!/_3$ Msamples/s. This sample rate centers the spectrum of the discrete-time signal at the quarter-sample-rate frequency. This reduces the resources required to perform the subsequent I/Q mixing and resampling operations [5]. At the A/D converter output, the number of samples per (over-the-air) bit is

$$N' = \frac{93\,{}^1\!/_3}{10.4} = \frac{350}{39}. \tag{6}$$

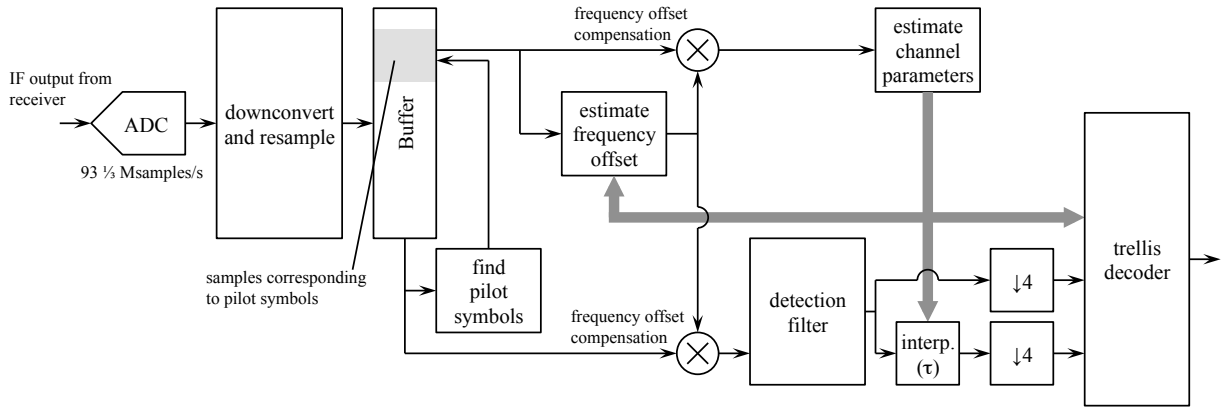

Figure 5: A block diagram of the prototype demodulator/decoder for space-time coded SOQPSK.

The resampling and I/Q mixing are combined using a polyphase filterbank that changes the sample rate by $78/175$. The result is the sequence sampled at 4 samples/bit denoted by

$$r(nT) = [h_0 s_0(nT - \tau_0) + h_1 s_1(nT - \tau_1)]\, e^{j\Omega_0 n} + w(nT) \tag{7}$$

where the sample time is $T = T_b/4$, $\Omega_0 = \omega_0 T$ rads/sample, and the $w(nT)$ are independent zero-mean complex-valued Gaussian random variables whose real and imaginary parts have variance σ^2. For the purposes of this development, suppose the first L_p samples correspond to the pilot bits in the received signal.

Pilot Detector Pilot detection is performed by correlating L_p samples of the data stored in the input buffer shown in Figure 5 with sampled versions of the SOQPSK signal corresponding to the two pilot bit sequences. Using the notation $p_0(nT)$ and $p_1(nT)$ to represent the samples of the SOQPSK signal corresponding to the pilot symbols used, the correlation functions are

$$\begin{aligned} \rho_0(n) &= \sum_{i=0}^{L_p-1} r((n+i)T) p_0^*(iT) \\ \rho_1(n) &= \sum_{i=0}^{L_p-1} r((n+i)T) p_1^*(iT) \end{aligned} \tag{8}$$

The samples of $p_0(nT)$ embedded in $r(nT)$ experience a phase shift due to the phase of h_0 and a delay by τ_0. The same observation applies to $p_1(nT)$ with h_1 and τ_1. For this reason, the magnitude squared of the two correlation functions is used. In the absence of a frequency offset $|\rho_0(n)|^2$ and $|\rho_1(n)|^2$ are compared to a threshold. If $|\rho_0(n_0)|^2$ and/or $|\rho_1(n_1)|^2$ exceed the threshold, then the samples corresponding to the pilot sequence have been found (at $n = n_0$ and $n = n_1$, respectively) and frame synchronization is established.

Because the pilot sequence is used to estimate the frequency offset at a later stage, the pilot detector described in the previous paragraph must be modified to account for uncompensated frequency offset. This can be accomplished by correlating each block of the received data by frequency

shifted versions of the pilot sequences. Experiments with the the pilot sequences show that both $|\rho_0(n_0)|^2$ and $|\rho_1(n_1)|^2$ are reduced to one-half their peak amplitudes at $f_0T_b \approx 1/300$ (or about 1/3 of one percent). This suggests correlating the blocks of the received data with a version of the pilot sequence frequency shifted by $\Delta f_0 T_b \approx 2/300$ cycles/bit is capable of producing a correlation peak at least one-half its maximum amplitude for frequency offsets in the range

$$\frac{1}{300} \leq f_0 T_b \leq \frac{3}{300}.$$

Motivated by this observation, define

$$\begin{aligned} p_0^-(nT) &= p_0(nT)e^{-j2\pi\Delta f_0 Tn} \\ p_0^+(nT) &= p_0(nT)e^{+j2\pi\Delta f_0 Tn} \\ p_1^-(nT) &= p_1(nT)e^{-j2\pi\Delta f_0 Tn} \\ p_1^+(nT) &= p_1(nT)e^{+j2\pi\Delta f_0 Tn}. \end{aligned} \tag{9}$$

These samples are used to perform pilot detection using the arrangement shown in Figure 6. Three correlators are used for each pilot sequence. Assuming sufficiently large value for $|h_0|$, one of the three correlator outputs operating on the shifted versions of $p_0(nT)$ exceeds the threshold. Similarly, if $|h_1|$ is sufficiently large, one of the shifted versions of $p_1(nT)$ exceeds the threshold.

Frequency Estimator The maximum likelihood frequency estimator is [6]

$$\hat{\Omega}_0 = \underset{\Omega}{\operatorname{argmax}} \left\{ \left| \sum_{n=0}^{L_p-1} r(nT) \left[h_0^* s_0^*(nT - \tau_0) + h_1^* s_1^*(nT - \tau_1) \right] e^{-j\Omega_0 n} \right|^2 \right\}. \tag{10}$$

In words, the maximum likelihood estimate is the value of Ω_0 that maximized the periodogram of the sequence

$$r(nT) \left[h_0^* s_0^*(nT - \tau_0) + h_1^* s_1^*(nT - \tau_1) \right]$$

for $0 \leq n < L_p$. Note that the estimate $\hat{\Omega}_0$ depends on the channel parameters h_0, h_1, τ_0, τ_1. Estimates of these values are used in place of the true values. There is no closed form solution. Consequently, the maximum likelihood estimate is found using a search.

Channel Estimator The best way to understand the channel estimator is to use a vector-matrix formulation. Stacking the elements $r(nT)$, $w(nT)$, $s_0(nT - \tau_0)$, and $s_1(nT - \tau_1)$ into column vectors forms

$$\mathbf{r} = \begin{bmatrix} r(0) \\ r(T) \\ \vdots \\ r((L_p - 1)T) \end{bmatrix}, \qquad \mathbf{w} = \begin{bmatrix} w(0) \\ w(T) \\ \vdots \\ w((L_p - 1)T) \end{bmatrix}, \tag{11}$$

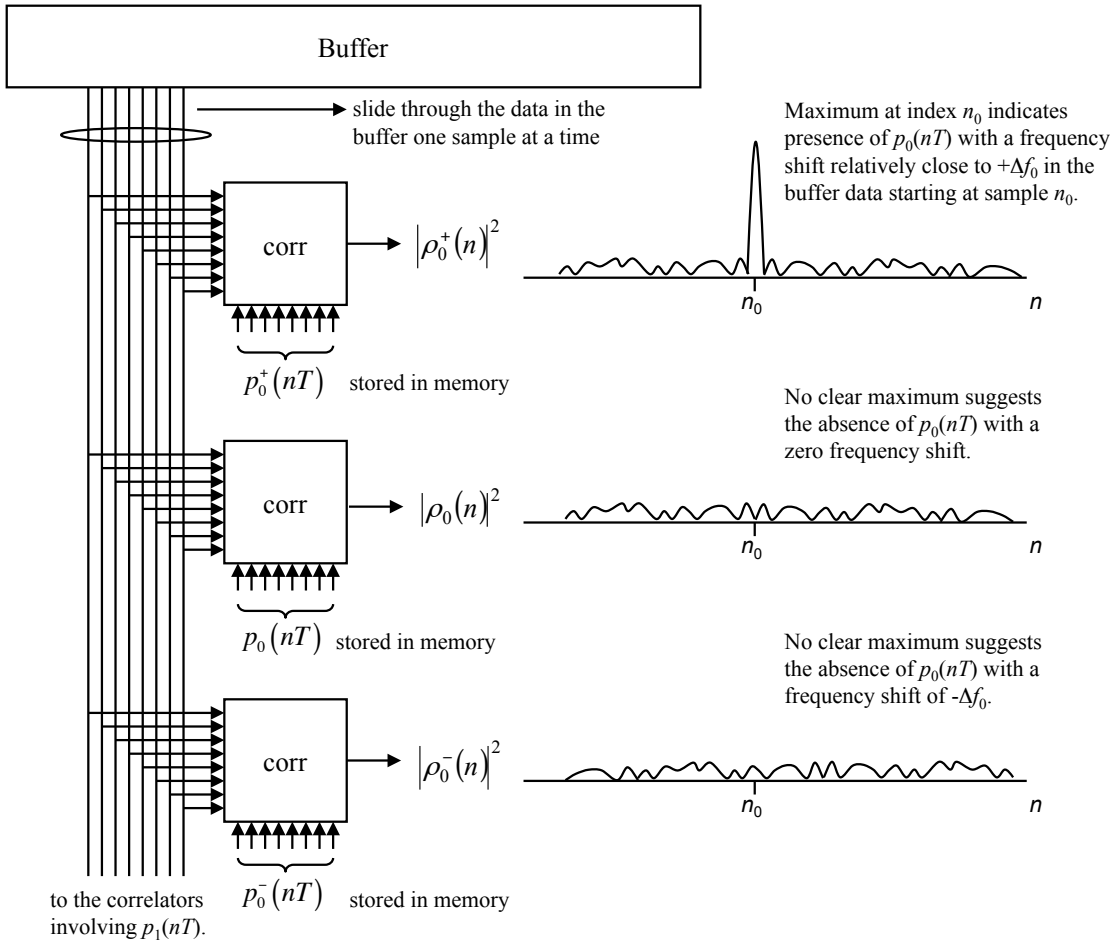

Figure 6: A pilot detector based on correlations using frequency shifted version of the pilot sequences.

$$\mathbf{s}_0(\tau_0) = \begin{bmatrix} s_0(-\tau_0) \\ s_0(T-\tau_0) \\ \vdots \\ s_0((L_p-1)T-\tau_0) \end{bmatrix}, \qquad \mathbf{s}_1(\tau_1) = \begin{bmatrix} s_1(-\tau_1) \\ s_1(T-\tau_1) \\ \vdots \\ s_1((L_p-1)T-\tau_1) \end{bmatrix}. \tag{12}$$

Assuming the frequency offset has been completely removed, the vector of received samples may be expressed as

$$\mathbf{r} = h_0\mathbf{s}_0(\tau_0) + h_1\mathbf{s}_1(\tau_1) + \mathbf{w}. \tag{13}$$

This expression may be compacted a bit more using by defining the matrix $L_p \times 2$ matrix $\mathbf{S}(\boldsymbol{\tau})$

$$\mathbf{S}(\boldsymbol{\tau}) = \begin{bmatrix} \mathbf{s}_0(\tau_0) & \mathbf{s}_1(\tau_1) \end{bmatrix} \quad \text{for} \quad \boldsymbol{\tau} = \begin{bmatrix} \tau_0 \\ \tau_1 \end{bmatrix} \tag{14}$$

and the 2×1 vector $\mathbf{h}$

$$\mathbf{h} = \begin{bmatrix} h_0 \\ h_1 \end{bmatrix}. \tag{15}$$

Using these definitions, (13) may be expressed as

$$\mathbf{r} = \mathbf{S}(\boldsymbol{\tau})\mathbf{h} + \mathbf{w}. \tag{16}$$

The maximum-likelihood estimator is [7]

$$\hat{\boldsymbol{\tau}} = \underset{\boldsymbol{\tau}}{\operatorname{argmin}} \left\{ \left| \left[\mathbf{I} - \mathbf{S}(\boldsymbol{\tau}) \left(\mathbf{S}^{\mathcal{H}}(\boldsymbol{\tau})\mathbf{S}(\boldsymbol{\tau}) \right)^{-1} \mathbf{S}^{\mathcal{H}}(\boldsymbol{\tau}) \right] \mathbf{r} \right|^2 \right\} \tag{17}$$

$$\hat{\mathbf{h}} = \left(\mathbf{S}^{\mathcal{H}}(\hat{\boldsymbol{\tau}})\mathbf{S}(\hat{\boldsymbol{\tau}}) \right)^{-1} \mathbf{S}^{\mathcal{H}}(\hat{\boldsymbol{\tau}})\mathbf{r}. \tag{18}$$

A search is required to find the solution (17). Since this search is performed in hardware, efficient evaluation of the argument of (17) for arbitrary values of $\boldsymbol{\tau}$ is not possible. The workaround is to precompute components of the argument of (17) at quantized values of τ_0 and τ_1 and store those values in memory. These stored values are used by the search to find the solution (17). An example of the search algorithm is illustrated in Figure 7. The figure shows a contour plot of the object function $F(\boldsymbol{\tau})$ evaluated at 64 discrete values for τ_0 and τ_1. The earch algorithm searches the contours to find the minimum. The minimum value is shown by the point and dashed lines in Figure 7.

Space-Time Decoding After the frequency offset has been estimated and removed from the received samples and the channel estimates have been computed, space-time decoding is performed. The first step in space-time decoding is the application of a detection filter. Note that in the prototype demodulator, the detection filter operates at 4 times the bit rate. The detection filter output must be sampled at two different T_b-spaced intervals, offset by $\tau = \tau_1 - \tau_0$ as illustrated in Figure 5. The detection filter outputs $x(iT_b)$ and $x(iT_b + \tau)$ are compared with samples of the detection filter response to space-time coded SOQPSK. In the following description, we use

$$y(t; b_{-5}, \ldots, b_0, \ldots, b_5)$$

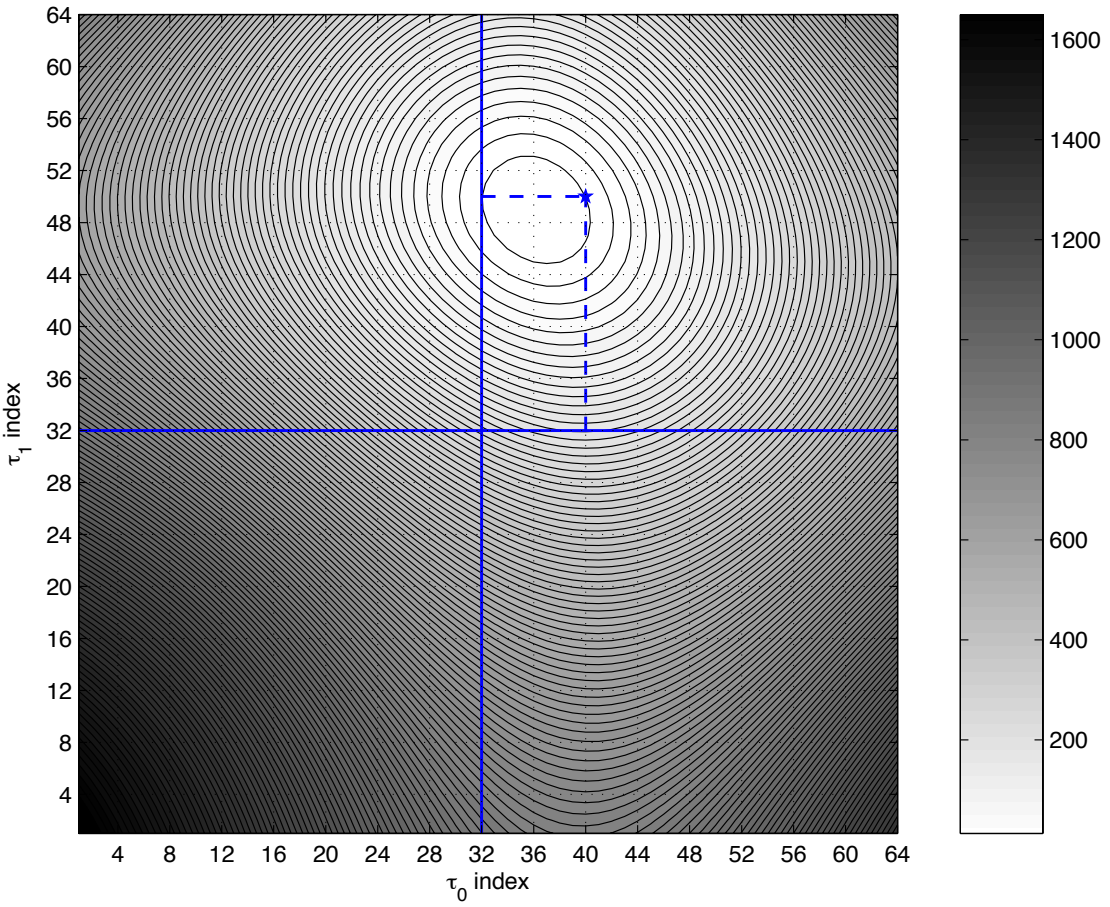

Figure 7: An illustration of the contour plot of the argument of (17) for 64 discrete values of τ_0 and τ_1.

to be the detection filter response to SOQPSK for the 11-bit sequence $b_{-5}, \ldots, b_0, \ldots, b_5$. The bit indexes are somewhat arbitrary but are used to convey to the reader the notion of a "middle bit" in the XTCQM representation of SOQPSK and that the XTCQM representation of SOQPSK consists of $2^{11} = 2048$ states. Using an averaging technique described in [8], approximations for $y(t;\cdot)$ that require fewer states may be used in the detection process. In the prototype demodulator, the 32-state approximation

$$\tilde{y}(t; b_{-2}, b_{-1}, b_0, b_1, b_2)$$

was used. As explained in the previous section, the space-time code groups the bits into blocks of 4. There are 8 pairs of detection filter outputs that contain terms dependent on the block of bits $b_{4k-6}, b_{4k-5}, b_{4k-4}, b_{4k-3}$. The last four pairs define a subtrellis block that repeats in the overall trellis. The least squares estimate can be expressed as

$$\hat{b}_{4k-6}, \hat{b}_{4k-5}, \hat{b}_{4k-4}, \hat{b}_{4k-3} = \underset{b_{4k-6},\ldots,b_{4k-3}}{\operatorname{argmin}} \left\{ \sum_{i=0}^{3} \left[\left| \Delta_{4k+i}^{(0)} \right|^2 + \left| \Delta_{4k+i}^{(\tau)} \right|^2 \right] \right\} \tag{19}$$

where

$$\begin{aligned}
\Delta_{4k}^{(0)} &= x(4kT_b) - h_0\tilde{y}(0; b_{4k-2}, b_{4k-3}, \overline{b}_{4k-4}, b_{4k-5}, b_{4k-6}) \\
&\quad - h_1\tilde{y}(-\tau; b_{4k}, \overline{b}_{4k-5}, b_{4k-6}, b_{4k-3}, b_{4k-4}) && (20) \\
\Delta_{4k}^{(\tau)} &= x(4kT_b + \tau) - h_0\tilde{y}(\tau; b_{4k-2}, b_{4k-3}, \overline{b}_{4k-4}, b_{4k-5}, b_{4k-6}) \\
&\quad - h_1\tilde{y}(0; b_{4k}, \overline{b}_{4k-5}, b_{4k-6}, b_{4k-3}, b_{4k-4}) && (21) \\
\Delta_{4k+1}^{(0)} &= x((k+1)T_b) - h_0\tilde{y}(T_b; b_{4k-2}, b_{4k-3}, \overline{b}_{4k-4}, b_{4k-5}, b_{4k-6}) \\
&\quad - h_1\tilde{y}(T_b - \tau; b_{4k}, \overline{b}_{4k-5}, b_{4k-6}, b_{4k-3}, b_{4k-4}) && (22) \\
\Delta_{4k+1}^{(\tau)} &= x((4k+1)T_b + \tau) - h_0\tilde{y}(T_b + \tau; b_{4k-2}, b_{4k-3}, \overline{b}_{4k-4}, b_{4k-5}, b_{4k-6}) \\
&\quad - h_1\tilde{y}(T_b; b_{4k}, \overline{b}_{4k-5}, b_{4k-6}, b_{4k-3}, b_{4k-4}) && (23) \\
\Delta_{4k+2}^{(0)} &= x((4k+2)T_b) - h_0\tilde{y}(0; \overline{b}_{4k}, b_{4k-1}, b_{4k-2}, b_{4k-3}, \overline{b}_{4k-4}) \\
&\quad - h_1\tilde{y}(-\tau; b_{4k-2}, b_{4k+1}, b_{4k}, \overline{b}_{4k-5}, b_{4k-6}) && (24) \\
\Delta_{4k+2}^{(\tau)} &= x((4k+2)T_b + \tau) - h_0\tilde{y}(\tau; \overline{b}_{4k}, b_{4k-1}, b_{4k-2}, b_{4k-3}, \overline{b}_{4k-4}) \\
&\quad - h_1\tilde{y}(0; b_{4k-2}, b_{4k+1}, b_{4k}, \overline{b}_{4k-5}, b_{4k-6}) && (25) \\
\Delta_{4k+3}^{(0)} &= x((4k+3)T_b) - h_0\tilde{y}(T_b; \overline{b}_{4k}, b_{4k-1}, b_{4k-2}, b_{4k-3}, \overline{b}_{4k-4}) \\
&\quad - h_1\tilde{y}(T_b - \tau; b_{4k-2}, b_{4k+1}, b_{4k}, \overline{b}_{4k-5}, b_{4k-6}) && (26) \\
\Delta_{4k+3}^{(\tau)} &= x((4k+3)T_b + \tau) - h_0\tilde{y}(T_b + \tau; \overline{b}_{4k}, b_{4k-1}, b_{4k-2}, b_{4k-3}, \overline{b}_{4k-4}) \\
&\quad - h_1\tilde{y}(T_b; b_{4k-2}, b_{4k+1}, b_{4k}, \overline{b}_{4k-5}, b_{4k-6}). && (27)
\end{aligned}$$

The corresponding trellis depends on the relationship between τ_0 and τ_1. The trellis for the case $\tau_0 > \tau_1$ and $\tau_0 < \tau_1$ are plotted in [9].

Hardware Implementation The prototype demodulator is shown in Figure 8. The input is a filtered 70 MHz IF output from a separate receiver (not shown) whose output level is -10 dBm.

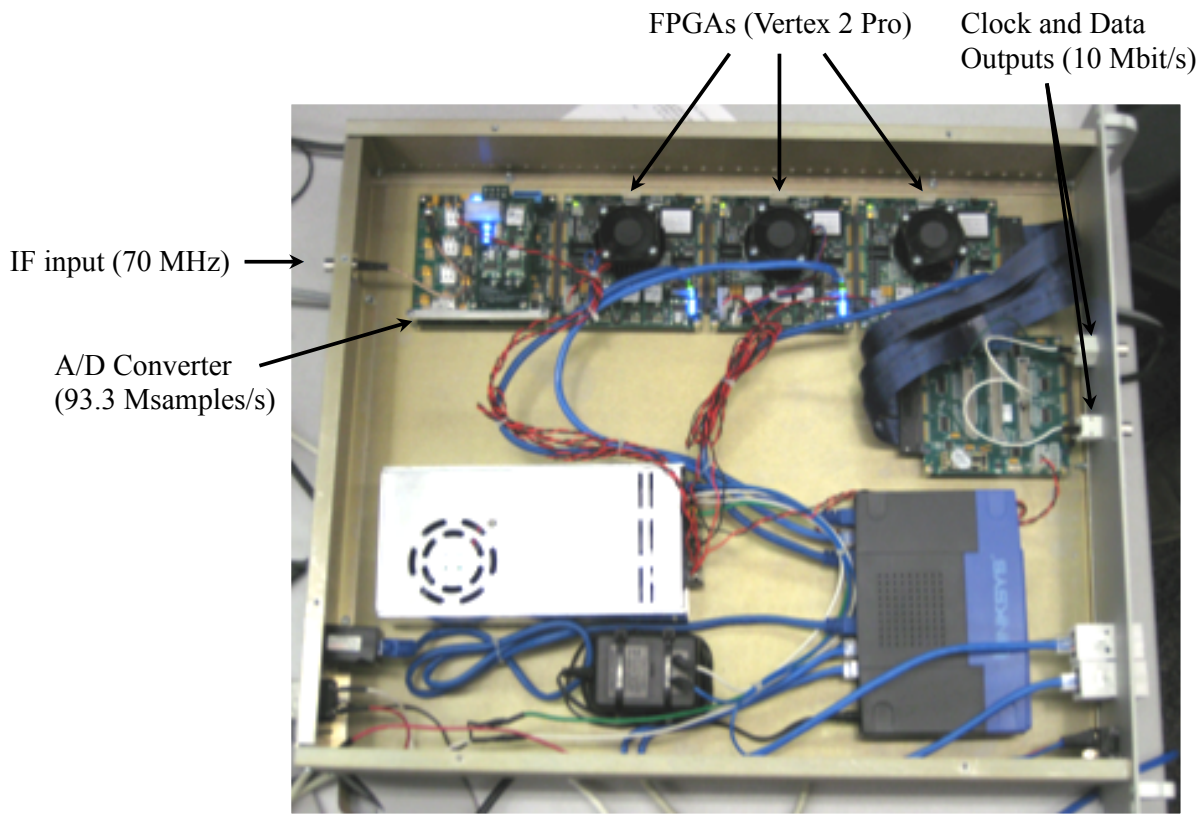

Figure 8: An image of the prototype space-time demodulator.

The A/D converters samples the signal as described above. Three Virtex-2 Pro FPGAs were used for the digital downconverter and resampler, the pilot sequence detector, the frequency offset and channel estimators, and the trellis-based space-time decoder. TTL-level clock and data outputs were derived from the output buffer in the last stage of the FPGA. The prototype modulator was capable operating at a variable data rate. The prototype demodulator, however, operated at a fixed data rate of 10 Mbits/s (this corresponds to an over-the-air data rate of 10.4 Mbits/s).

Laboratory tests of the system were conducted to assess the space-time coded system in a benign additive noise environment. A block diagram of the test setup used for the tests is shown in Figure 9. 2-transmit-to-1-receive-antenna propagation was imitated using a combiner applied to attenuated versions of the two RF outputs from the STC transmitter. Variable attenuators were used so that the impact of different signal strengths could be measured. Calibrated noise was added using the FastBit noise and interference test set.

The corresponding BER test results are plotted in Figure 10. For reference, the BER test results for two SOQPSK-TG demodulators in a cable test involving one transmitter and one receiver are also included. For the space-time coded system, a number of different scenarios are tested as indicated in the legend. Even though the plot is cluttered, the main point is clear: in a benign laboratory environment, the bit error rate performance of prototype demodulator in a 2-transmit/1-receive antenna configuration is comparable to that of existing SOQPSK demodulators in a traditional

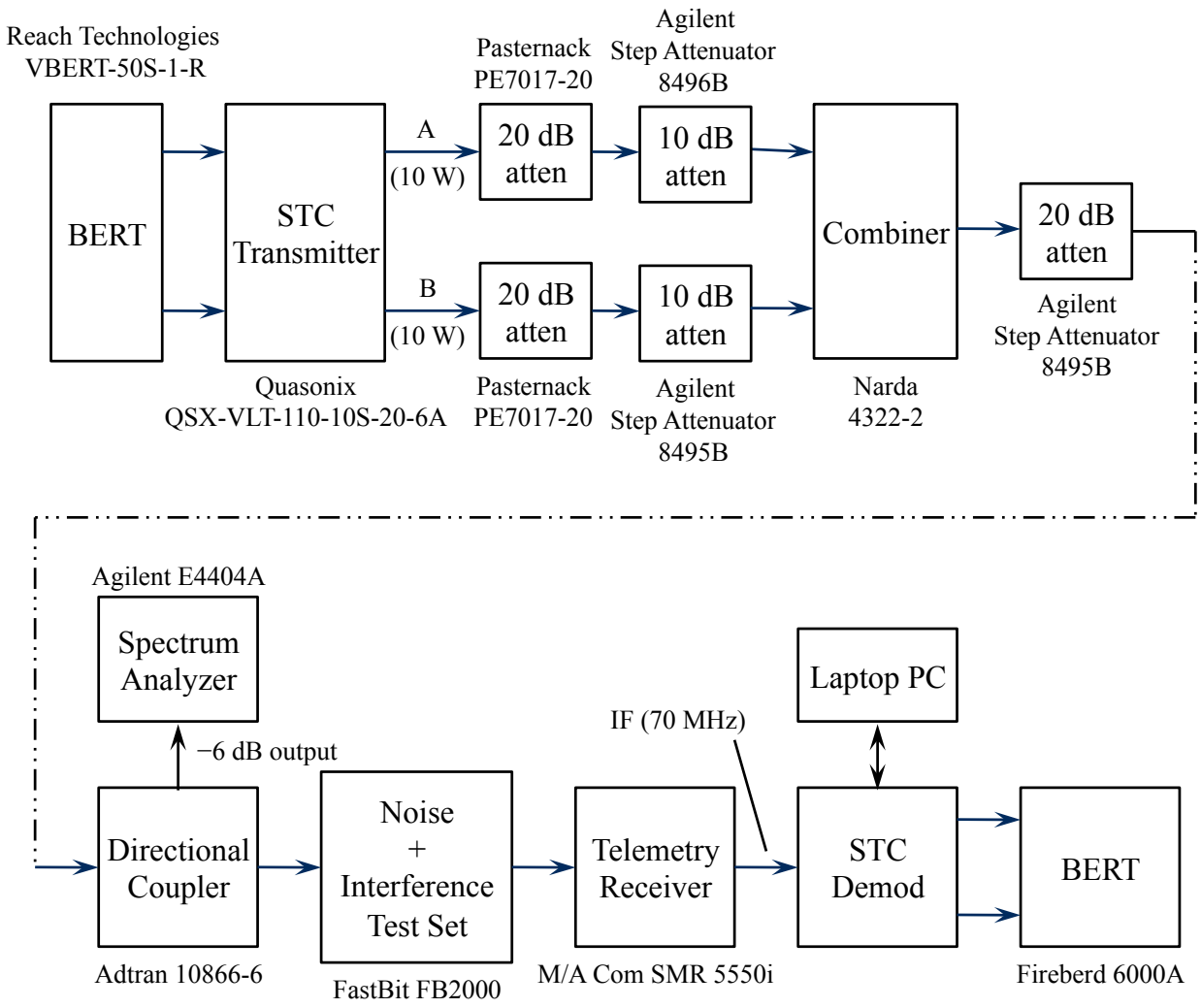

Figure 9: A block diagram of the laboratory BER test of the space-time coded system.

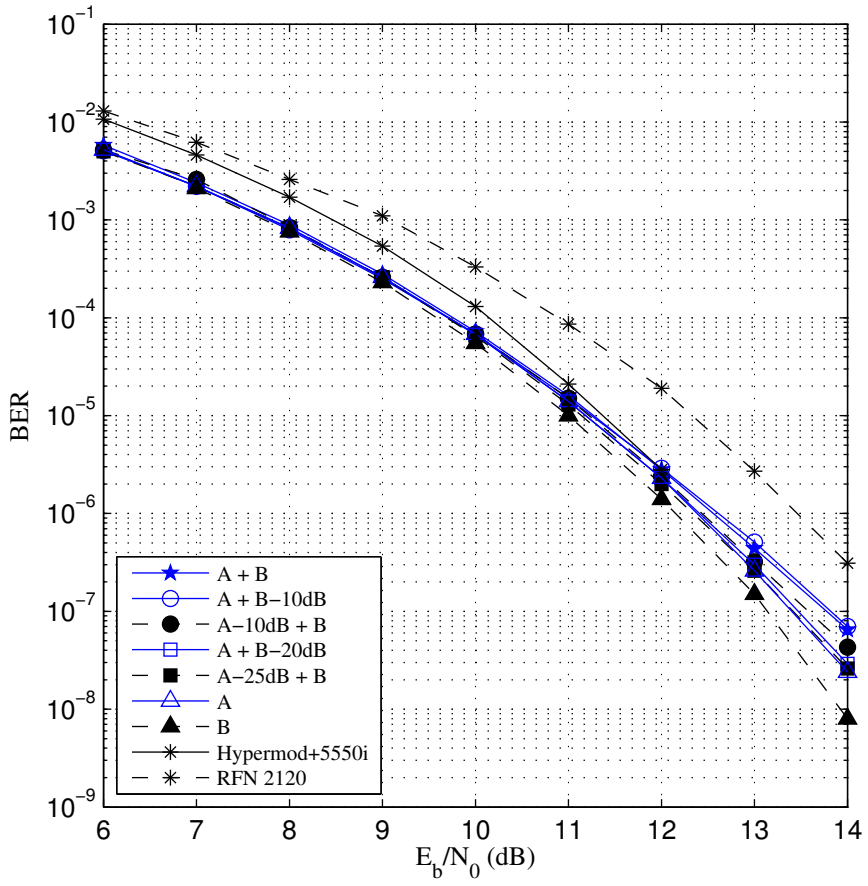

Figure 10: The BER test results for the prototype demodulator/decoder for several different 2-transmit/1-receive antenna configurations. For reference, the bit error rate performance of two existing SOQPSK demodulators operating in a 1-transmit/1-receive antenna configuration are also shown. The over-the-air bit rate for the space-time coded test is 10.4 Mbits/s. The over-the-air bit rate for the traditional SOQPSK link is 10 Mbits/s.

1-transmit/1-receive configuration.

CONCLUSIONS

This paper described the design and implementation of a prototype transmitter and a prototype demodulator/decoder for space-time coded SOQPSK-TG for aeronautical telemetry. The design exercise showed that the space-time coding concept can be reduced to hardware. The laboratory bit error rate tests showed that the performance of the prototype demodulator in a 2-transmit/1-receive antenna configuration is comparable to that of existing SOQPSK demodulators in a 1-transmit/1-receive antenna configuration. What remains to be shown is the performance of the prototype demodulator in a real operational environment. That is the subject of the companion paper [4].

ACKNOWLEDGEMENTS

The author acknowledges the help of Mr. Kip Temple (Air Force Flight Test Center) who performed the BER tests reported in this paper and Mr. Glen Wolf (Delphi Research, Inc., Air Force Flight Test Center) who assembled the test hardware.

This work was supported by the Test Resource Management Center (TRMC) Test and Evaluation Science and Technology (T&E/S&T) Program through a grant to BYU from the US Air Force Flight Test Center under contract FA9302-05-C-0001 and from the Army PEO STRI Contracting Office under contract W900KK-09-C-0016.

REFERENCES

[1] M. Jensen, M. Rice, T. Nelson, and A. Anderson. Orthogonal dual-antenna transmit diversity for SOQPSK in aeronautical telemetry channels. In *Proceedings of the International Telemetering Conference*, San Diego, CA, October 2004.

[2] T. Nelson, M. Rice, and M. Jensen. Experimental results with space-time coding using FQPSK. In *Proceedings of the International Telemetering Conference*, Las Vegas, NV, October 2005.

[3] M. Jensen, M. Rice, and A. Anderson. Aeronautical telemetry using multiple-antenna transmitters. *IEEE Transactions on Aerospace and Electronic Systems*, 43(1):262–272, January 2007.

[4] M. Rice and K. Temple. Space-time coding for aeronautical telemetry: Part II — experimental results. In *Proceedings of the International Telemetering Conference*, Las Vegas, NV, October 2011.

[5] M. Rice. *Digital Communications: A Discrete-Time Approach*. Pearson Prentice-Hall, Upper Saddle River, NJ, 2009.

[6] D. Rife and R. Boorstyn. Single-tone parameter estimation from discrete-time observations. *IEEE Transactions on Information Theory*, 20(5):591 – 598, September 1974.

[7] A. Swindlehurst. Time delay and spatial signature estimation using known asynchronous signals. *IEEE Transactions on Signal Processing*, 46(2):449–462, February 1998.

[8] T. Nelson, E. Perrins, and M. Rice. Near optimal common detection techniques for shaped offset QPSK and Feher's QPSK. *IEEE Transactions on Communications*, 56(5):724 – 735, May 2008.

[9] M. Rice. Final report: Prototype design of aeronautical telemtry space-time decoder system, 2010. US Air Force Flight Test Center.